13th AIAA/ISSMO Multidisciplinary Analysis Optimization Conference
13 - 15 September 2010, Fort Worth, Texas

AIAA 2010-9200

Aerothermodynamic Shape Optimization of Hypersonic Entry Aeroshells

John E. Theisinger*, Dr. Robert D. Braun†, and Dr. Ian G. Clark‡
Georgia Institute of Technology, Atlanta, Georgia, 30332-0150

Previous work by the authors has focused on the optimization of entry aeroshell shapes based solely on objectives related to aeroshell geometry and hypersonic aerodynamic performance. This multi-objective optimization framework has been extended to include the impact of hypersonic aerothermodynamics – that is, aerodynamic heating is now considered alongside the previously-developed objectives. The methodology for performing aerothermodynamic analyses has been adapted from research that has demonstrated the ability to obtain an approximate three-dimensional heating distribution using axisymmetric analyses by matching certain similarity criteria. In the current work, axisymmetric solutions are obtained by coupling Newtonian inviscid solutions with axisymmetric boundary-layer relations that provide an estimate of heat flux. Non-uniform rational B-spline surfaces are used to represent aeroshell shapes. In order to maintain continuity with the previous work, the current aerothermodynamic analysis method is applied to the Mars Science Laboratory mission, in which a heat-rate-minimization objective is traded against objectives to maximize drag-area, static stability, and volumetric efficiency. Two-objective optimizations are performed to highlight major trends and tradeoffs between heat rate and the other three objectives. Results are compared to the baseline 70-degree sphere-cone aeroshell.

Nomenclature

A	=	reference area
C_DA	=	drag-area (= D/q_∞)
C_mAl	=	pitching moment per unit freestream dynamic pressure (= m/q_∞)
C_p	=	pressure coefficient
D	=	drag force
H	=	mean curvature
L/D	=	lift-to-drag ratio
L	=	lift force
l	=	reference length
m	=	mass or pitching moment
q	=	dynamic pressure
$\dot{q}$	=	heat flux (W/cm^2)
$\dot{Q}$	=	heat rate (W)
Re	=	Reynolds number
S	=	surface area
T	=	temperature
V	=	volume or velocity
α	=	angle of attack
β	=	ballistic coefficient
γ	=	ratio of specific heats
ρ	=	density
η_V	=	volumetric efficiency

* Graduate Research Assistant, Daniel Guggenheim School of Aerospace Engineering, AIAA Student Member.
† David and Andrew Lewis Associate Professor of Space Technology, Daniel Guggenheim School of Aerospace Engineering, AIAA Associate Fellow.
‡ Visiting Assistant Professor, Daniel Guggenheim School of Aerospace Engineering, AIAA Member.

Subscripts

ref	=	reference quantity
∞	=	freestream
w	=	wall
wet	=	wetted

I. Introduction

AEROSHELLS are designed to deliver payloads safely through a planetary atmosphere, protecting the payload from the high aerodynamic heating and loads encountered during hypersonic entry, descent, and landing (EDL). The aeroshell is designed to provide this function with minimum possible mass so that useful landed mass can be maximized.

An aeroshell generally consists of a forebody, which faces the flow, and a backshell, which completes the encapsulation of the payload. The forebody must accommodate the majority of the aerodynamic heating encountered by the aeroshell during hypersonic entry. For this purpose, a thermal protection system (TPS) is designed to withstand anticipated heat fluxes and heat loads – quantities that roughly define the TPS material and thickness, respectively. Therefore, an objective to minimize TPS mass attempts to minimize heat load while constraining heat fluxes to remain within TPS material limitations.

In their seminal work, Allen and Eggers[1] concluded that the total heat load for a hypersonic ballistic missile would be minimized when the shape produced a minimum ratio of frictional drag to total drag. To illustrate this conclusion, consider a comparison between a slender and blunt aeroshell shape. For a slender aeroshell shape, the frontal shock wave is oblique to the flow and possibly attached to the body. This shock is relatively weak and the kinetic energy of the flow remains high within the shock layer. As this flow reaches the surface, viscous dissipation within the boundary layer results in large shear stresses and convective heat fluxes at the surface. That is, the shear force, or frictional drag, is the dominant source of total drag. For a blunt aeroshell shape, the shock wave is strong and detached. Across this shock, a large portion of the kinetic energy of the flow is converted into thermal energy (or high-temperature flow). Because the shock layer is relatively thick, much of this flow is then carried away before reaching the surface. In this case, pressure drag is the dominant source of total drag and the ratio of frictional drag to total drag is greatly reduced in comparison to the slender aeroshell. Overall, less thermal energy reaches the surface and the heat fluxes are reduced relative to the slender body case.

Total drag is also an important factor in determining aerodynamic heating when considering its effect on trajectory: a higher drag causes the aeroshell to decelerate at higher, less-dense portions of the atmosphere, resulting in a more benign heating environment. Traditionally, the ballistic coefficient (β) is the aeroshell performance parameter that embodies this principle, relating inertial and drag forces as shown in Eq. (1).

$$\beta = \frac{m}{C_D A} \tag{1}$$

It is desirable to minimize β in order to maximize this deceleration. Minimizing β can be carried out by designing the aeroshell to have maximum drag-area (C_DA), as shown by Eq. (1). Based on the conclusion of Allen and Eggers, it is the pressure component of C_DA that should be maximized. The addition of lift, or *L*/*D*, can provide a similar reduction in aerodynamic heating as the aeroshell is able to maintain a higher altitude (lower density) at a given velocity in the trajectory. Note, however, that increasing *L*/*D* is likely to conflict with the objective to reduce β due to competing demands on C_DA. Other significant sources of aerodynamic heating that are related to aeroshell shape include transition to turbulence and entropy swallowing. Both effects increase temperature gradients within the boundary layer, leading to increased heat flux at the surface.

Previous work by the authors[2] focused on aeroshell shape optimization from the perspective of geometry and hypersonic aerodynamics. That is, focus was placed on objectives related to lift, drag, stability, and overall structural and packaging efficiency. The current work extends consideration to hypersonic aerothermodynamics. Specifically, a technique has been implemented to approximate the heat flux distributions over aeroshell shapes under consideration. From such distributions, heat fluxes are easily monitored and the rate of heat input is calculated by integrating heat flux over the aeroshell surface. These quantities are then included during the optimization of aeroshell shapes. The chosen analysis method is of a low level of fidelity and is both computationally efficient and appropriate for the conceptual analysis of candidate aeroshell shapes.

While both convective and radiative sources of heating are important in aeroshell shape design, the current work focuses on convective heating only. Furthermore, the primary function of this study is to assess trends in aerodynamic heating relating to aeroshell shape and to assess tradeoffs against other design objectives. The chosen analysis method thus facilitates relative comparisons between aeroshell shapes.

II. Methodology

The current work is separated into three main components: shape parameterization, aerothermodynamic analysis, and optimization. The following sections detail each component and discuss how these components were integrated to perform multi-objective aeroshell shape optimization.

A. Shape Parameterization

The proper choice of shape parameterization is that which yields an appropriate mix of design freedom and computational efficiency. In terms of numerical optimization, it is most computationally efficient to keep the number of design variables to a minimum; however, more design freedom typically requires a larger number of variables. Because aeroshell shapes can vary in complexity based on design requirements, the goal here is to select a shape parameterization that permits sufficient design freedom with a manageable number of variables.

Spline surfaces provide significant flexibility with a reasonably small number of design variables. The most flexibility can be obtained by representing aeroshell shapes using non-uniform rational B-spline (NURBS) surfaces[3]. Furthermore, NURBS surfaces provide the ability to represent both analytic quadric surfaces and arbitrary free-form surfaces. Surfaces are defined by specifying the locations of control points which form a bidirectional control net. Further control is achieved through specification of weights (placed on each control point) and knot values (which define the parameter rectangle over which each control point influences the surface). The NURBS formulation also has two important geometric properties: 1) the convex hull property, which ensures that the surface lies within the convex hull created by the control points, and 2) the local support property, which ensures that each control point only affects a localized region of the surface. Given these two properties, the designer can readily predict the surface shape based on its control net, as the control net forms a planar polyhedral approximation to the surface. Overall, the NURBS surface formulation provides a high degree of shape control and is an intuitive framework for interactive shape design

The surface parameterization used in this work is shown in Fig. 1 and was employed in the previous work by the authors[2]. A cubic × quadratic degree surface provides the desired amount of design flexibility for roughly 20 design variables, including control point locations, their weights, and α. Knot values are held fixed. Constraints are imposed on control point locations such that resulting shapes are convex. Only half of the control net needs to be defined since all aeroshells in this investigation are symmetric across the pitch plane. Control points are distributed axially from the apex of the forebody to the apex of the backshell, totaling five different convex axial control point profiles that define one half of the aeroshell. The forebody and backshell apex can be moved anywhere vertically along the forebody and backshell, respectively.

Once defined, the control net is mirrored across the pitch plane to form a complete aeroshell surface. The fact that NURBS can exactly represent quadric surfaces provides an advantage in terms of constraint enforcement. For example, in the present work each control point cross-section is constrained within a circular envelope, presuming a cylindrical launch vehicle shroud. Once a maximum length and radius are defined, control point placement and weight specifications yield a complete aeroshell surface.

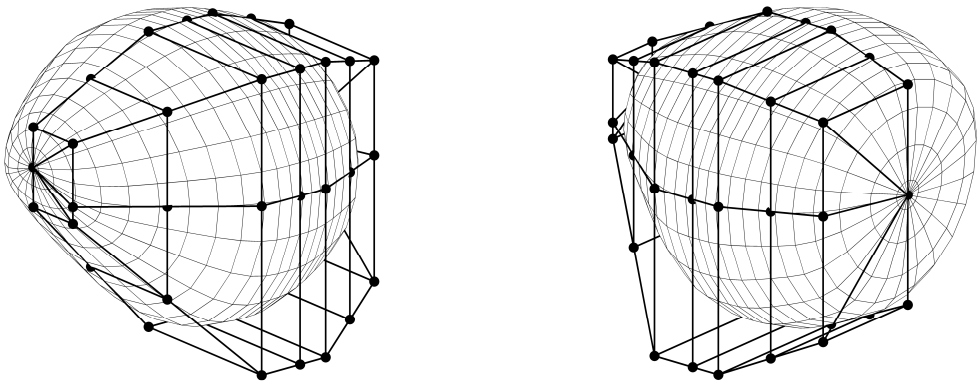

Figure 1. NURBS aeroshell surface parameterization.

B. Hypersonic Aerothermodynamics

The hypersonic aerothermodynamic characteristics of entry aeroshells can be estimated through a variety of numerical methods. Incorporating any single method in the process of shape optimization requires careful consideration, in that each method represents a unique tradeoff between computational effort and fidelity. Since the purpose of this study is to explore the trends and tradeoffs between multiple objectives over a fairly large design space, a method requiring minimal computational effort is required.

The most rapid estimates for heat flux distributions over general 3D aeroshell shapes are made using low-fidelity aerothermodynamic methods. These methods generally employ a two-layer model, splitting the flowfield into a layer of inviscid outer flow and a viscous boundary-layer near the surface. Such methods are appropriate when the traditional boundary-layer assumptions apply (i.e., large Re_∞ and thin boundary-layer); however, it has been shown that the assumption of a thin boundary-layer may be erroneous for very large Mach number flows[4]. In such situations, the two-layer approximation is inappropriate – the entire shock layer should instead be handled simultaneously; however, this level of analysis is beyond the scope of the current low-fidelity study.

1. *Approximate 3D Aerothermodynamic Analyses*

Brykina, Rusakov, and Shcherbak[5] developed a method to approximate the heating distribution over general 3D bodies using only axisymmetric solutions. An approximate, analytical solution for heat flux was derived from the 3D thin viscous shock layer equations. This solution showed heat flux to depend primarily on two parameters: 1) the inclination of the body surface with respect to the freestream flow (θ), and 2) the ratio $\mathrm{Re}/H\cos(\theta)$ where Re and H are the local Reynolds number and mean curvature, respectively. Hence, if these two parameters are matched between two bodies, their heat fluxes will be approximately equal.

The purpose of the method is then to generate axisymmetric bodies with heat flux distributions which are approximately equivalent to heat flux distributions along the 3D body. Following the approach of Brykina and Scott[6], these equivalent axisymmetric bodies (EABs) are generated from meridians defined by the intersection of the surface of the 3D body and a plane that passes through the geometric (or Newtonian) stagnation point and that rotates about the freestream velocity vector (see Fig. 2). Given a 3D meridian, the geometry of the corresponding EAB is defined completely by the distribution in θ along that meridian. To satisfy the second parameter, the resulting heat flux distribution along the EAB is scaled by the factor $\sqrt{H_{3D}/H_{EAB}}$ to provide an estimate for the heat flux distribution along the 3D meridian. This process is then repeated for many EABs to obtain desired coverage over the 3D body.

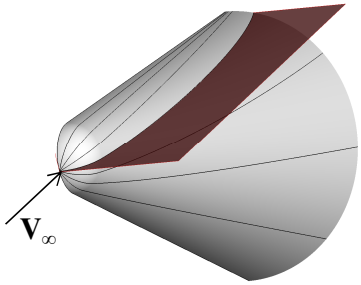

Figure 2. 3D body with velocity plane used to define meridians.

In addition to not requiring any sort of 3D solution, this approach has the advantage that the process of EAB generation and subsequent aerothermodynamic analysis can be carried out completely in parallel. This independence in EAB aerothermodynamic analysis also provides a clear pathway for the eventual inclusion of multiple levels of analysis fidelity. That is, differing levels of fidelity can be applied to individual EABs as deemed necessary by formulated empirical or heuristic guidelines. Having its roots in thin viscous shock layer theory, the method is only applicable to attached flow and is best applied only to surface area of the aeroshell that is wetted by the flow (S_{wet}). In terms of Newtonian flow theory[4], S_{wet} corresponds to non-shadowed regions of the aeroshell surface. In this work, the number of EABs will be held fixed at 19, corresponding to a meridian spacing of 10 deg in angle about the half-body. Due to this, certain geometric features will inevitably be overlooked during EAB analysis – a deficiency that is likely to be exploited by the optimizer. This lack of complete coverage is a drawback of the method that can potentially be alleviated through increasing the number or meridians or by developing other schemes to distribute meridians.

2. *Axisymmetric Aerothermodynamic Analyses*

For the hypersonic flows encountered by aeroshells during planetary entry, Newtonian impact theory provides an appropriate estimate of inviscid surface pressure distributions[4]. The remaining inviscid flowfield properties can be estimated by computing the entropy behind a normal shock at the given freestream conditions, and then assuming isentropic expansion from the stagnation point to these local Newtonian pressures. The direction of local velocity is determined by assuming that the component of the freestream velocity vector normal to the surface is destroyed and the resulting velocity direction is tangent to the surface. This inviscid flowfield represents the edge conditions for a boundary-layer solution that can be used to estimate heat rates.

Rather than carry out a complete boundary-layer solution, simplified relations for surface heat flux are applied based on the assumption of local similarity. Such methods apply most accurately when edge properties are slowly

varying. Here, local similarity is applied along generated EABs. Along each EAB, a locally axisymmetric boundary-layer assumption is made in which axisymmetric boundary-layer relations developed by Zoby, et al.[7] are applied to compute heat flux. Compressibility effects are accounted for through the use of a reference enthalpy. Laminar or turbulent heating can also be computed with this method, but this study focuses exclusively on laminar flow.

C. Multi-Objective Aeroshell Shape Optimization

The previous work by the authors[2] focused on aeroshell shape optimization based on three conflicting objectives: C_DA, static stability [$(C_mAl)_\alpha$], and volumetric efficiency (η_V). The particular application was based on the Mars Science Laboratory (MSL) mission and incorporated requirements on L/D and volume (V), and constraints on overall aeroshell size. In that work, both single- and multi-objective optimizations were carried out using genetic algorithms (GAs). Using the low-fidelity aerothermodynamic method described above, this same methodology can be applied to include aerodynamic heating as a design objective.

1. Geometric Objectives and Constraints

Certain objectives and constraints are computed directly from the aeroshell geometry. Volume and surface area (S) are easily computed once the aeroshell geometry is defined and generated using NURBS surfaces. A requirement on V is then checked directly, while additional objectives can be derived from combinations of V and S.

Payload packaging efficiency refers to the distribution of V (and therefore payload) enclosed by the aeroshell surface and can be quantified as a ratio between V and S. A high payload packaging efficiency is defined as the ability to enclose a prescribed payload (indicating a certain V requirement) with minimum structural mass (a limitation on S). This statement contains the assumption that aeroshell structural mass is directly proportional to S – with a proportionality constant equal to an average structural areal density. This simplified model is used in conceptual aeroshell sizing to estimate structural mass from a known S and an areal density based on historical data[8]. The parameter that embodies this definition of packaging efficiency is the volumetric efficiency (η_V), defined in Eq. (2)[9].

$$\eta_V = 6\sqrt{\pi}\frac{V}{S^{3/2}} \tag{2}$$

Note that η_V is maximized at unity for a sphere, which is the aeroshell shape with the best η_V. As such, slender aeroshell shapes generally have a lower η_V and therefore a higher structural mass than blunt aeroshells (for a given V). Additionally, lower η_V indicates a poorer ability to package payload into the aeroshell.

2. Aerothermodynamic Objectives and Constraints

Once an aeroshell surface and α have been specified, hypersonic aerodynamic characteristics are determined using Newtonian theory. These characteristics include C_DA, $(C_mAl)_\alpha$, and L/D. Based on reasoning discussed in Ref. 2, the current motivation prescribes an optimization problem in which L/D is used as a constraint, C_DA is maximized, and static stability is maximized by minimizing the quantity $(C_mAl)_\alpha$.

Additional objectives and constraints are obtained from the hypersonic aerothermodynamic analysis that provides an approximate estimate of the heat flux distribution. A maximum heat flux, $\dot{q}_{\max}$, can be determined and used as a constraint typically defined by a particular choice in TPS material. In order to capture the instantaneous influence of the entire heating distribution, the heat flux $(\dot{q})$ is integrated over the entire forebody surface area to compute the overall heat rate, defined in Eq. (3). Such a quantity will be directly proportional to the overall TPS mass of the aeroshell.

$$\dot{Q} = \int_{S_{wet}} \dot{q} dS \tag{3}$$

3. Optimization

As in the previous work[2], the current optimization problem must handle multiple, conflicting objectives and has many different optimal solutions, each representing a particular compromise, or tradeoff, among these objectives. The population-based nature of evolutionary multi-objective algorithms enables many Pareto-optimal solutions to be obtained in a single execution, as opposed to methods that convert the multi-objective optimization problem into a single-objective optimization problem and produce only one Pareto-optimal solution per execution.

The Isight®[10] software package provides the non-dominated sorting GA (NSGA-II) for multi-objective optimization. Source code was developed in Fortran to perform NURBS aeroshell shape generation, EAB generation, and aerothermodynamic analysis. The resulting executable provides all objective and constraint evaluations. The design variables are the locations and weights of NURBS control points and α. The range of possible solutions is limited by constraints such as *L*/*D*, *V*, and overall size.

The NSGA-II is able to treat multiple objectives simultaneously. Initially, a random parent population is created and then sorted into successive non-dominated fronts based on their objective values. Each solution is assigned a rank equal to its non-dominated front. A crowding distance is computed within each front to differentiate between solutions of the same rank (a diversity-preserving operation). Genetic operations are then performed on the parent population to create an offspring population. The parent and offspring are combined (an elite-preserving operation) and the combined population is sorted and ranked. A new parent population is selected and the steps repeat until termination. The final result is a diverse set of Pareto-optimal solutions. Constraints are handled using binary tournament selection, during which two solutions are chosen from the population and either: 1) the best solution is selected from the two feasible solutions, 2) the one feasible solution is selected, or 3) the solution with the smallest constraint violation is selected from the two infeasible solutions.

III. Results

In keeping with previous work[2], The Mars Science Laboratory (MSL) aeroshell is used as a baseline with which to explore the capabilities developed in this work. Aerodynamic and geometric constraints are derived from published MSL geometry and mission requirements[11]. A NURBS representation of the MSL-derived aeroshell is shown in Fig. 3. It has a 70° sphere-cone forebody with a conical backshell and is intended to fly at a non-zero α, thereby producing an *L*/*D* of 0.24. There is a maximum-diameter constraint of 4.5 m dictated by the diameter of the launch vehicle fairing and the size of the integration and test facilities at the Jet Propulsion Laboratory. An aeroshell *V* requirement of approximately 20.2 m^3 was determined from the present MSL design. A maximum length constraint was determined based on the total length of the MSL aeroshell, which is approximately 2.84 m. Thus, an optimized aeroshell is required to fit within a 4.5-m-diameter × 2.84-m-length circular cylinder, have a *V* of approximately 20.2 m^3, and achieve an *L*/*D* of 0.24. All of these constraints are to be met by the multi-objective optimization problem. As described in the previous work[2], the use of equality constraints on *V* and *L*/*D* is too severe within the NSGA-II framework. Once again, each equality constraint is replaced by two inequality constraints. In this work, the *V* and *L*/*D* equality constraints were both relaxed by 10% of the original equality constraint value: *V* was constrained between approximately 20.2 m^3 and 22.3 m^3 and *L*/*D* was constrained between 0.24 and 0.264.

In order to highlight the tradeoffs associated with this particular application, the following four objectives were selected for aeroshell shape optimization: $\dot{Q}$, C_DA, $(C_mAl)_\alpha$, and η_V. The analytic baseline aeroshell shown in Fig. 3 was analyzed using the same aerothermodynamics analysis routine that would be employed for optimization. The freestream conditions correspond to a point 77.8 s in the MSL +3σ heat flux trajectory[11]. These conditions correspond to: V_∞ = 4.84 km/s, ρ_∞ = 1.27 x 10^{-3} kg/m^3, and T_∞ = 173 K. For simplicity, perfect gas analyses were performed with γ = 1.3 and wall temperature was held fixed at a value of 300 K.

Using the NURBS aeroshell shown in Fig. 3, the α_{trim} required to produce an *L*/*D* of 0.24 was first determined. At this value of α_{trim}, the $\dot{Q}$, C_DA, $(C_mAl)_\alpha$, and η_V were computed. These values serve as a baseline against which to compare solutions produced through optimization and are shown in Table 1. Also, $\dot{q}_{max}$ for the analytic baseline was calculated for use as a heating constraint during optimization.

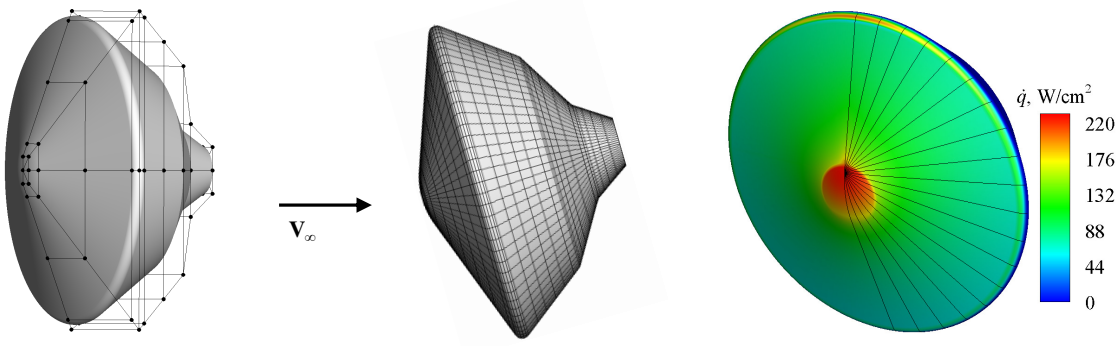

Figure 3. Baseline aeroshell, illustrating NURBS control net, surface grid, and heat flux distribution with 3D meridians used for aerothermodynamic analysis, α_{trim} = -16.2 deg.

Table 1. Objective and constraint values for baseline aeroshell.

Parameter	Value
$\dot{Q}$, W	7.894 x 10^6
C_DA, m^2	22.92
$(C_mAl)_\alpha$, m^3/rad	-14.14
η_V	0.7895
$\dot{q}_{max}$, W/cm^2	228.3
L/D	0.240
V, m^3	20.2

Since pairwise comparisons were made in Ref. 2 between the three objectives C_DA, $(C_mAl)_\alpha$, and η_V, the current work focused on investigating the trends and tradeoffs between $\dot{Q}$ and the these three objectives. Using the NSGA-II, sets of Pareto-optimal solutions were generated for these three pairs of objectives by performing two-objective optimizations. In addition to the constraints mentioned above, all designs were required to perform at least as well as the analytic baseline based on the two objectives under consideration (i.e., the values given in Table 1). For a given pair of objectives, resulting solutions therefore provide improvement relative to the analytic baseline in terms of those objectives and dominate it in the Pareto sense. The results for all three optimizations are shown in Fig. 4, with axes displaying the percent improvement in objective values relative to the baseline aeroshell.

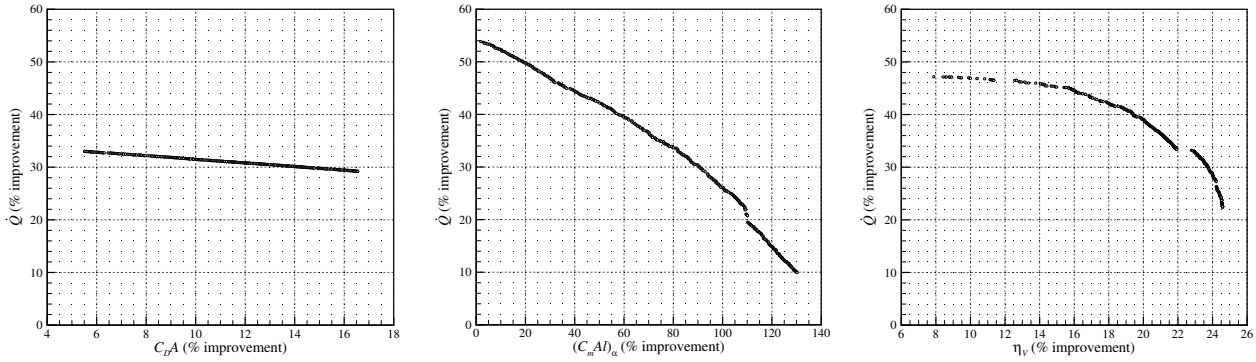

a) Minimize $\dot{Q}$ and maximize C_DA. **b) Minimize $\dot{Q}$ and minimize $(C_mAl)_\alpha$.** **c) Minimize $\dot{Q}$ and maximize η_V.**

Figure 4. Pareto-optimal solutions, shown as percent improvement from the baseline aeroshell.

Figure 5, 6, and 7 display comparisons between the bounding solutions taken from the Pareto fronts in Figs. 4a, 4b, and 4c, respectively. These bounding solutions represent the aeroshells that provide the greatest improvements in the pairs of objectives under consideration. Each of these figures diplay the aeroshell NURBS surface meshes and contour plots of C_p and $\dot{q}$, all placed at the corresponding α_{trim}.

Figure 5 displays a comparison between the bounding solutions taken from the Pareto front in Fig. 4a. Overall, the solutions along this Pareto front display a similar geometric character: a very blunt forebody with backshell almost entirely shadowed from the flow. A negative α_{trim} provides the necessary L/D and remains relatively constant over the entire Pareto front. The minimization of $\dot{Q}$ and maximization of C_DA has resulted in blunting of the forebody so as to decrease $\dot{q}$ and increase C_p, respectively. The $\dot{Q}$ and C_DA distributions confirm this behavior and are relatively invariant along this Pareto front. Because both $\dot{Q}$ and C_DA are quantities computed by integrating over S_{wet}, maximizing C_DA corresponds to maximizing S_{wet}, while minimizing $\dot{Q}$ corresponds to minimizing S_{wet}. Thus, S_{wet} is the primary source of tradeoff between this pair of objectives. In general, lower $\dot{Q}$ aeroshells have a smaller, elliptical cross-section while higher C_DA aeroshells have fully circular cross-sections that maximize the cross-sectional size constraint. The stagnation region of the forebody profile is slightly rounded to prevent violation of the $\dot{q}_{max}$ constraint since, for these geometries, $\dot{q}_{max}$ occurs at the stagnation point.

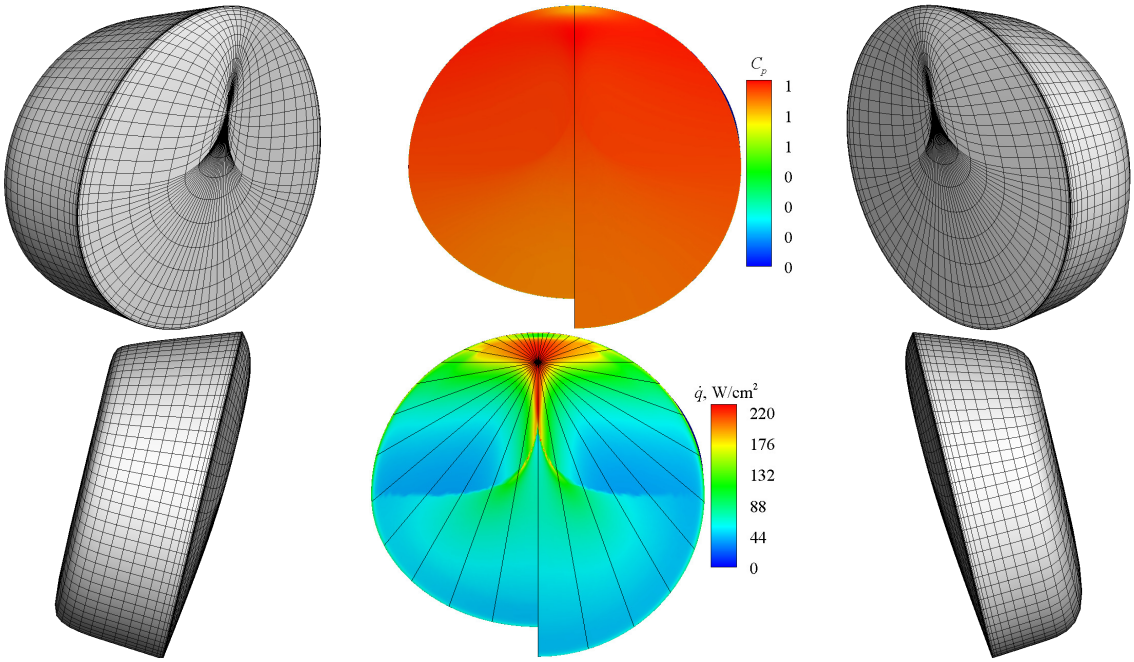

Figure 5. Aeroshells from Fig. 4a that exhibit greatest improvement in $\dot{Q}$ (left) and C_DA (right) with comparison of C_p and $\dot{q}$ contours (center).

Figure 6 displays a comparison between the bounding solutions taken from the Pareto front in Fig. 4b. Minimization of $\dot{Q}$ has again resulted in blunting; however this blunting is localized to the stagnation region. The remaining aeroshell surface is swept, or inclined at varying degrees, relative to the flow with relatively low $\dot{q}$. The interface between the blunt and swept regions is slightly rounded so as to prevent violation of $\dot{q}_{\max}$ constraint since $\dot{q}_{\max}$ occurs in this region for these geometries. The maximization of static stability has resulted in all the aeroshell volume being shifted forward into the wetted region, or forebody, of the aeroshell. The broad, flattened surfaces wetted by the flow serve to provide strong restoring moments and maximize the static stability. The lower, inclined surface provides the necessary *L*/*D* while the aeroshell maintains negligible α_{trim} across this Pareto front. There is again a slight tradeoff influenced by S_{wet}. Lower $\dot{Q}$ aeroshells have a smaller, elliptical cross-section with the upper surface largely shadowed from the flow. Aeroshells with high stability have fully circular cross-sections that maximize the cross-sectional size constraint and result in an upper surface that more inclined toward the flow.

Finally, Fig. 7 displays a comparison between the bounding solutions taken from the Pareto front in Fig. 4c. Once again, minimization of $\dot{Q}$ has produced geometries with a relatively large, blunted stagnation region as illustrated by the aeroshell with maximum improvement in $\dot{Q}$. This stagnation region becomes more rounded and S_{wet} increases as η_V increases (moving right along this Pareto front). The necessary *L*/*D* is provided by the inclined lower surface while the aeroshell maintains negligible α_{trim}. Most of the aeroshell surface is swept relative to the flow, with relatively low $\dot{q}$, and becomes cylindrical to provide higher η_V. As η_V continues to increase, a discontinuity in the Pareto front is encountered corresponding to a distinctive shift in both the aeroshell geometry and orientation (α_{trim}). At this point, the aeroshell is able to provide a discontinuous increase in η_V without an increase in $\dot{Q}$. The change is illustrated by the aeroshell with maximum improvement in η_V shown in Fig. 7. This aeroshell no longer has a large, flat stagnation region – the aeroshell remains blunt with respect to the flow through a relatively large, negative α_{trim} that both presents a low-curvature surface to the flow and provides the necessary *L*/*D*.

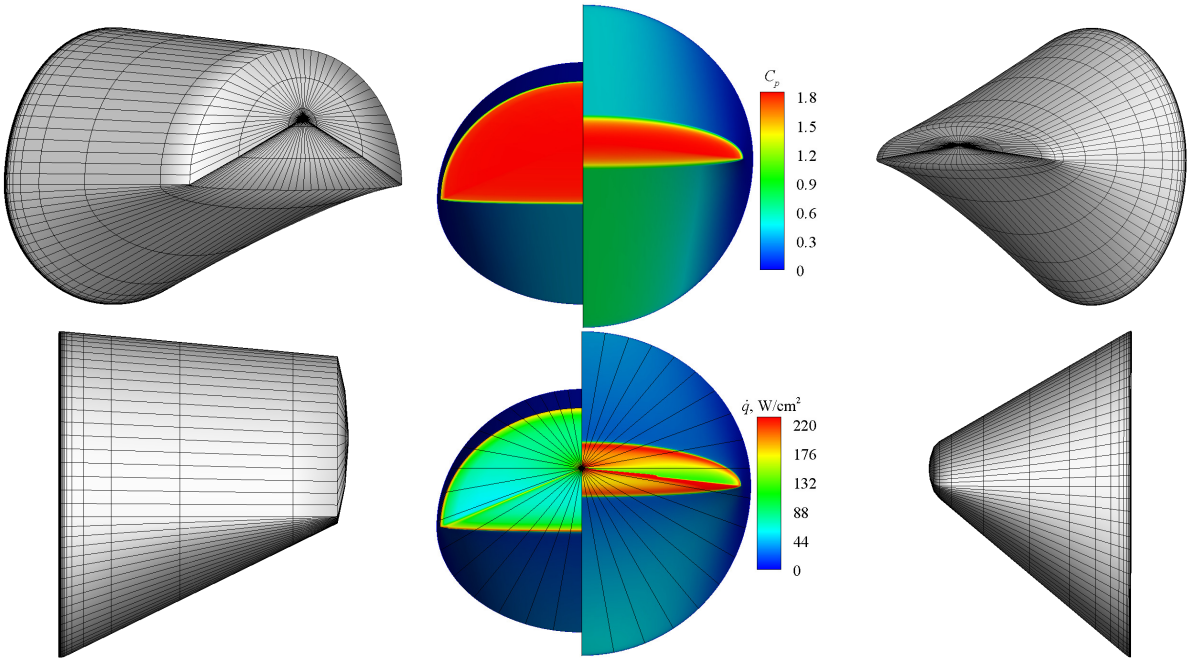

Figure 6. Aeroshells from Fig. 4b that exhibit greatest improvement in $\dot{Q}$ (left) and $(C_m A l)_a$ (right) with comparison of C_p and $\dot{q}$ contours (center).

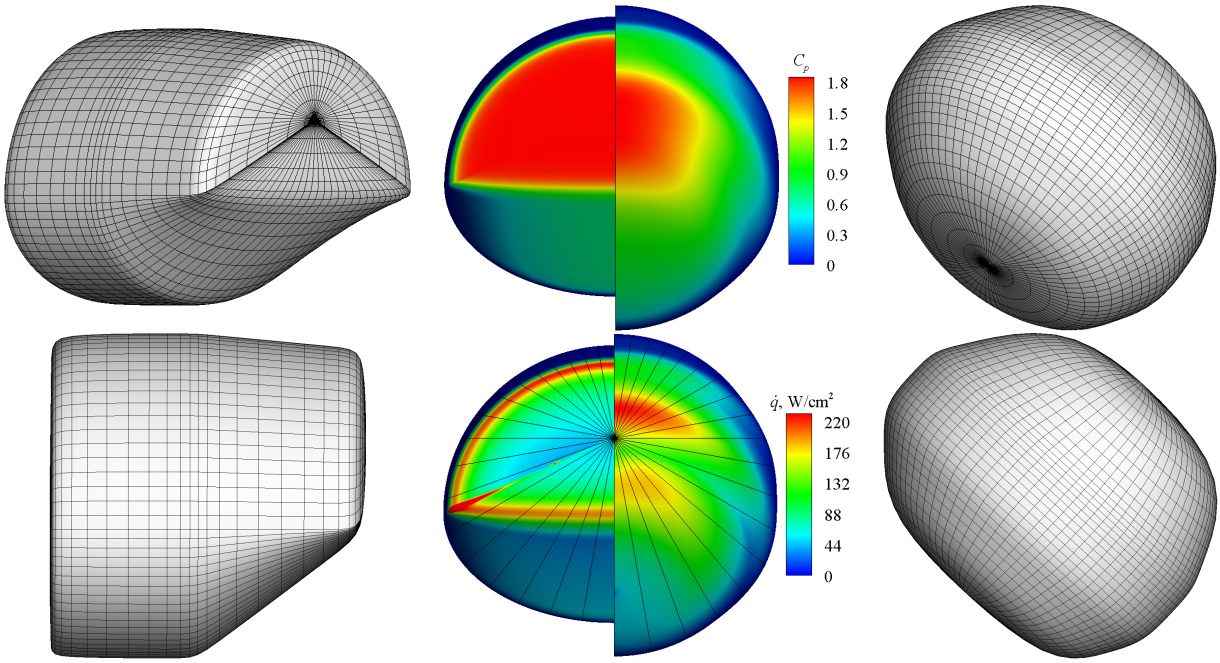

Figure 7. Aeroshells from Fig. 4c that exhibit greatest improvement in $\dot{Q}$ (left) and η_V (right) with comparison of C_p and $\dot{q}$ contours (center).

VI. Conclusions

A previously-developed multi-objective optimization framework has been extended to consider the impact of hypersonic aerothermodynamics. The non-uniform B-spline surface formulation is used to represent the aeroshell shapes because it allows for a wide diversity of aeroshell shapes while maintaining a relatively low number of control points (or design variables) for optimization.

The methodology for performing aerothermodynamic analyses has been adapted from research that demonstrates the ability to obtain an approximate three-dimensional heating distribution based on only axisymmetric analyses. These axisymmetric analyses are performed along equivalent axisymmetric bodies that have been generated from surface meridians extending away from the geometric stagnation point. By matching certain similarity criteria, these axisymmetric solutions provide an estimate for the heating on the three-dimensional body. In this work, axisymmetric solutions have been obtained by coupling Newtonian inviscid solutions with an axisymmetric boundary-layer relation that provides an estimate of heat flux.

The method has been applied to the Mars Science Laboratory mission, in which a heat-rate-minimization objective was traded against objectives to maximize drag-area, static stability, and volumetric efficiency. Three two-objective optimizations were performed to highlight major trends and tradeoffs. Results revealed solutions that offer improvement in these objectives relative to the analytic 70° sphere-cone, which has been employed by all U.S. robotic Mars missions. These sets of Pareto-optimal solutions also served to highlight the fundamental tradeoffs between heat rate and drag-area, static stability, and volumetric efficiency. In general, minimization of the heat rate corresponds to minimization of overall wetted surface area, increased blunting of the stagnation region, and increased sweep in the remaining wetted surface area of the aeroshell. Local reductions in surface curvature may also be required to avoid violating constraints on maximum heat flux.

Acknowledgments

This research was supported through a contract with the NASA ARMD Fundamental Aeronautics Program Hypersonics Project for High Mass Mars Entry System research. The input and guidance provided by Mark Schoenenberger of NASA Langley Research Center is greatly appreciated.

References

[1] Allen, H. J. and Eggers, A. J., Jr., "A Study of the Motion and Aerodynamic Heating of Ballistic Missiles Entering the Earth's Atmosphere at High Supersonic Speeds," NACA TR-1381, 1958.

[2] Theisinger, J. E. and Braun, R. D., "Multi-Objective Hypersonic Entry Aeroshell Shape Optimization," *Journal of Spacecraft and Rockets*, Vol. 46, No. 5, 2009, pp. 957-966.

[3] Piegl, L. and Tiller, W., *The NURBS Book*, 2nd ed., Springer-Verlag, Berlin, 1997, pp. 128-136.

[4] Anderson, J. D., *Hypersonic and High Temperature Gas Dynamics*, 2nd ed., AIAA Education Series, AIAA, Reston, VA, 2006, pp. 54-63, 70-71, 73-74, 292, 299-300, 326-327, 341-346.

[5] Brykina, I. G., Rusakov, V. V., and Shcherbak, V. G., "A Method of Determining the Heat Fluxes and Friction in Three-Dimensional Problems of Hypersonic Streamline Flow Using Two-Dimensional Solutions," *Dokl. Akad. Nauk. SSSR*, Vol. 316, 1991, pp. 62-66.

[6] Brykina, I. G. and Scott, C. D., "An Approximate Axisymmetric Viscous Shock Layer Aeroheating Method for Three-Dimensional Bodies," NASA TM-98-207890, May 1998.

[7] Zoby, E. V., Moss, J. N., and Sutton, K., "Approximate Convective-Heating Equations for Hypersonic Flows," *Journal of Spacecraft and Rockets*, Vol. 18, No. 1, 1981, pp. 64-70.

[8] Dyke, E. R., "Planetary Probe Mass Estimation Tool Development and its Application to Titan Aerocapture," AIAA Paper 2003-4956, July 2003.

[9] Hankey, W. L., and Elliott, G. A., "Hypersonic Lifting Body Optimization," *Journal of Spacecraft and Rockets*, Vol. 5, No. 12, Dec. 1968, pp. 1463-1467.

[10] Isight, Software Package, Ver. 4.5, Dassault Systèmes Simulia Corp., Providence, RI, 2010.

[11] Edquist, K. T., Dyakonov, A. A., Wright, M. J., and Tang, C. Y., "Aerothermodynamic Environments Definition for the Mars Science Laboratory Entry Capsule," AIAA Paper 2007-1206, Jan. 2007.